Supplementary Materials: Pyridine-2,6-Dicarboxylic Acid Esters ($pydicR_2$) as O,N,O-Pincer Ligands in Cu^{II} Complexes

Katharina Butsch, Aaron Sandleben, Maryam Heydari Dokoohaki, Amin Reza Zolghadr and Axel Klein

Contents:

Supporting Figures

Figure S1. View on the crystal and molecular structures of $pydic(IPh)_2$ in *P*bca.

Figure S2. View on the crystal structure of $[Cu(OH_2)_6][\{Cu(pydic)\}_2(\mu\text{-}Cl)_2]$ in *P*1.

Figure S3. CVs of $(HNEt_3)[Cu(pydicMe_2)Cl_3]$ and $(HNEt_3)[Cu(pydicPh_2)Cl_3]$.

Figure S4. Absorption spectra of $[\{Cu(pydic(IPh)_2)Cl\}_2(\mu\text{-}Cl)_2]$.

Figure S5. Absorption spectra of $(HNEt_3)[Cu(pydicMe_2)Cl_3]$ and $(HNEt_3)[Cu(pydicPh_2)Cl_3]$.

Figure S6. Oxidative UV-vis spectroelectrochemistry of $[\{Cu(pydic(IPh)_2)Cl\}_2(\mu\text{-}Cl)_2]$.

Figure S7. Oxidative and reductive UV-vis spectroelectrochemistry of $(HNEt_3)[Cu(pydicPh_2)Cl_3]$.

Figure S8. DFT-calculated (B3LYP/6-31+G(d,p) level) contour plots of the frontier molecular orbitals of $(HNEt_3)[Cu(pydicMe_2)Cl_3]$ and $(HNEt_3)[Cu(pydicPh_2)Cl_3]$.

Figure S9. Electrostatic potential maps of $(HNEt_3)[Cu(pydicMe_2)Cl_3]$ in solvent media.

Figure S10. Electrostatic potential maps of $(HNEt_3)[CuCl_3(pydicPh_2)Cl_3]$ in solvent media.

Supporting Tables

Table S1. Crystal structure and refinement data of copper complexes and the ligand $pydic(IPh)_2$.

Table S2. DFT-calculated structure parameters for $[Cu(pydic(IPh)_2)Cl_2]$ and $[\{Cu(pydic(IPh)_2)Cl\}_2(\mu\text{-}Cl)_2]$.

Table S3. DFT-calculated structure parameters for $(HNEt_3)[Cu(pydicR_2)Cl_3]$ (R = Me or Ph) in the gas phase.

Table S4. DFT-calculated structure parameters for $(HNEt_3)[Cu(pydicR_2)Cl_3]$ (R = Me or Ph) in CH_2Cl_2 as solvent.

Table S5. DFT-calculated structure parameters for $(HNEt_3)[Cu(pydicR_2)Cl_3]$ (R = Me or Ph) in acetone as solvent.

Table S6. DFT-calculated structure parameters for $(HNEt_3)[Cu(pydicR_2)Cl_3]$ (R = Me or Ph) in MeCN as solvent.

Table S7. DFT-calculated structure parameters for $(HNEt_3)[Cu(pydicR_2)Cl_3]$ (R = Me or Ph) in DMF as solvent.

Table S8. DFT-calculated second-order perturbation energies $E^{(2)}$ (kJ/mol) of selected orbital interactions in $(HNEt_3)[Cu(pydicPh_2)Cl_3]$ in the gas phase and solvents.

Experimental Information

Structure solution and description of structural details of $pydic(IPh)_2$.

Structure solution and description of structural details of $[Cu(OH_2)_6][\{Cu(pydic)\}_2(\mu\text{-}Cl)_2]$.

Supporting Figures:

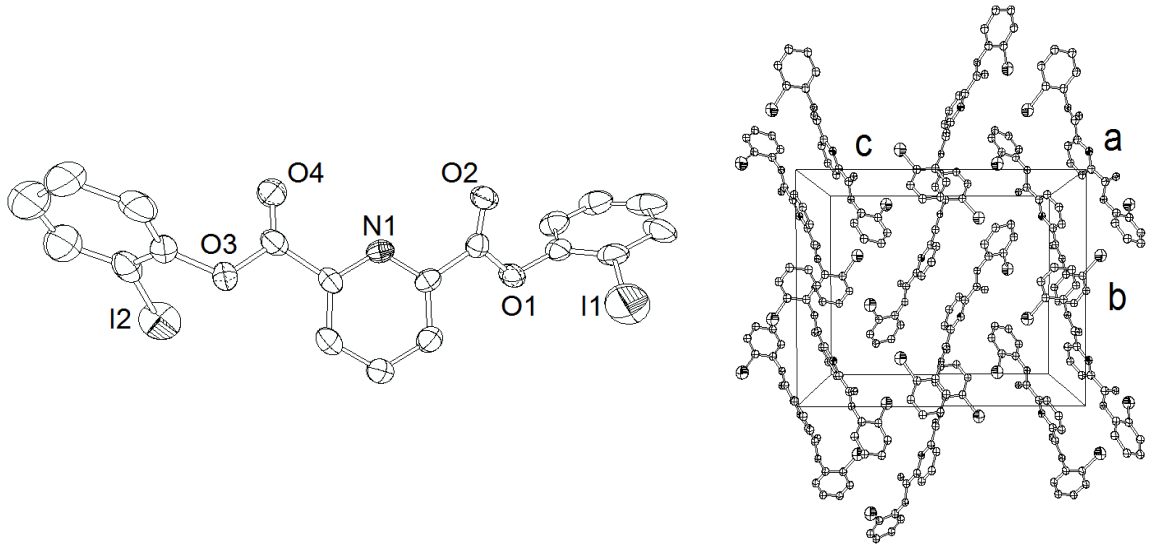

Figure S1. View on the crystal structure of pydic(IPh)$_2$ in *P*bca along the *a* axis (left); ORTEP representation at 50% probability level of the molecular structure; H atoms were omitted for clarity.

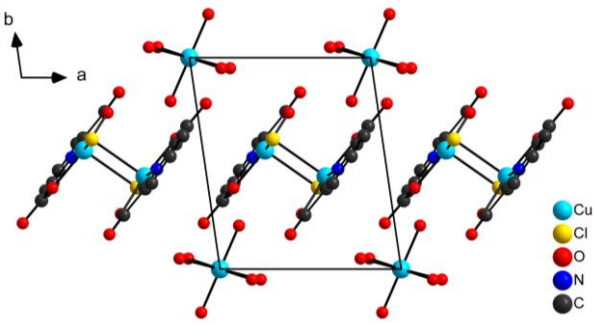

Figure S2. View on the crystal structure of [Cu(OH$_2$)$_6$][{Cu(pydic)}$_2$(μ-Cl)$_2$] in $P\bar{1}$ along the *c* axis.

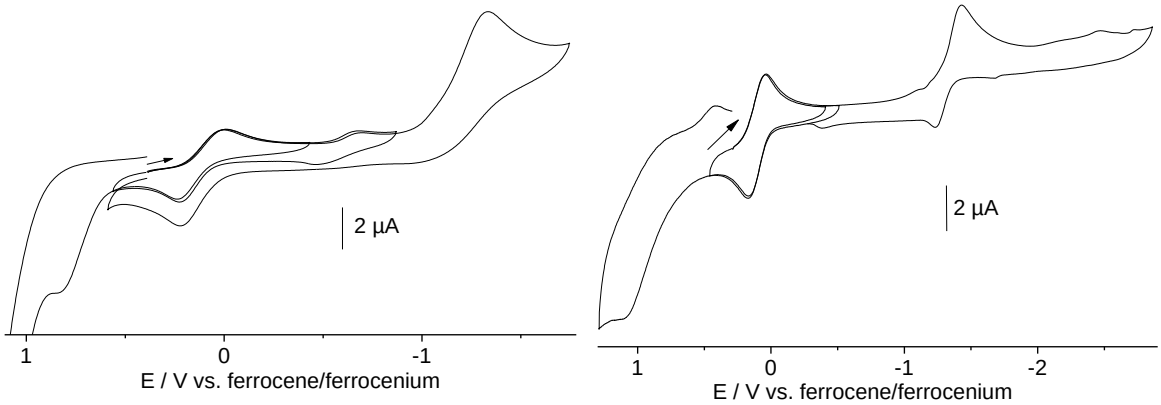

Figure S3. Cyclic voltammogramms of (HNEt$_3$)[Cu(pydicMe$_2$)Cl$_3$] (left) and (HNEt$_3$)[Cu(pydicPh$_2$)Cl$_3$] (right) in MeCN/^{n}Bu$_4$NPF$_6$ at 298 K with 100 mV/s scan rate.

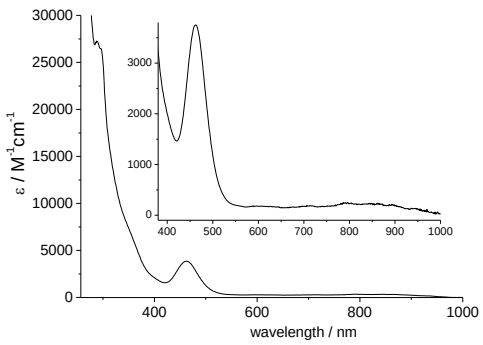

Figure S4. UV-vis absorption spectra of [{Cu(pydic(IPh)$_2$)Cl}$_2$(μ-Cl)$_2$] in MeCN.

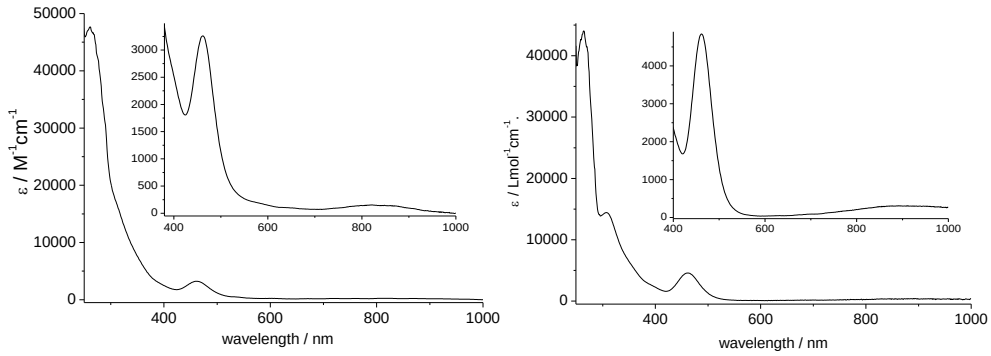

Figure S5. UV-vis absorption spectra of (HNEt$_3$)[Cu(pydicMe$_2$)Cl$_3$] (left) and (HNEt$_3$)[Cu(pydicPh$_2$)Cl$_3$] (right) in MeCN.

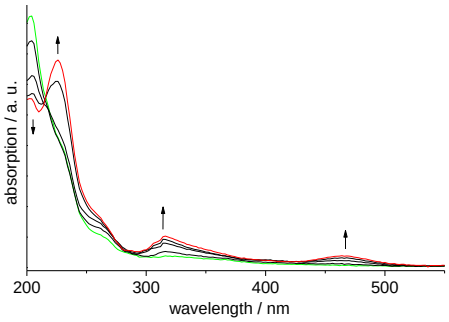

Figure S6. UV-vis absorption spectra recorded upon oxidative spectroelectrochemistry 0 to 1.5 V of [{Cu(pydic(IPh)$_2$)Cl}$_2$(μ-Cl)$_2$] in MeCN/^{n}Bu$_4$NPF$_6$ solution. Note that starting at 0 V means starting from the reduced form [{Cu(I)(pydic(IPh)$_2$)Cl}$_2$(μ-Cl)$_2$]$^{2-}$.

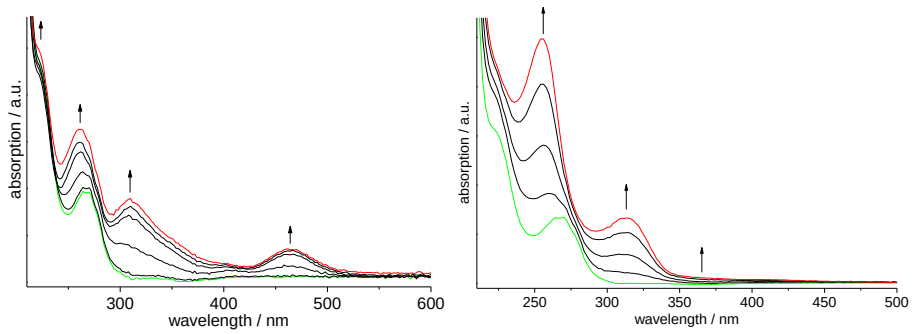

Figure S7. UV-vis absorption spectra of (HNEt$_3$)[Cu(pydicPh$_2$)Cl$_3$] recorded upon oxidative spectroelectrochemistry from 0 to 1.5 V (left) and reductive spectroelectrochemistry from 0 to –1,5 V (right) in MeCN/^{n}Bu$_4$NPF$_6$ solution. Note that starting at 0 V means starting from the reduced form [Cu(I)(pydicPh$_2$)Cl$_3$]$^{2-}$.

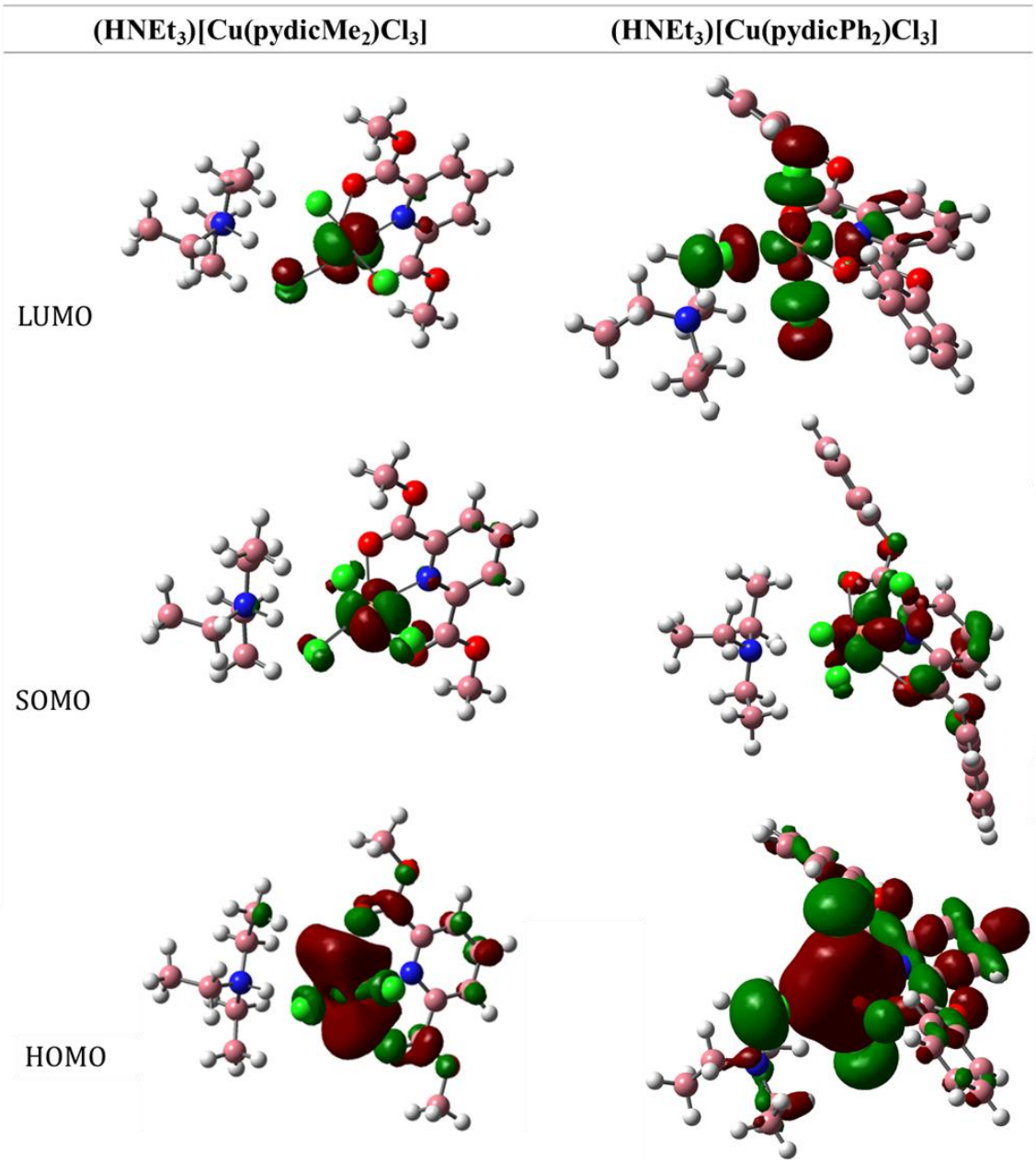

Figure S8. DFT-calculated (B3LYP/6-31+G(d,p) level) contour plots of the frontier molecular orbitals (HOMO = highest occupied molecular orbital; SOMO = singly occupied molecular orbital; LUMO = lowest unoccupied molecular orbital) of $(HNEt_3)[Cu(pydicMe_2)Cl_3]$ (left) and $(HNEt_3)[Cu(pydicPh_2)Cl_3]$ (right).

Although using the same basis set, the results for the frontier orbitals HOMO, SOMO, and LUMO are slightly different for the two complexes. For the $pydicPh_2$ derivative higher orbital contributions of the chlorido ligands to the frontier orbitals were found. Unfortunately, the resolution of the EPR spectra (Figure 8 in the manuscript), especially the lacking hyper fine splitting (coupling to the ^{63}Cu (69.17%) and ^{65}Cu (30.83%) nuclei both with $I = 3/2$) discloses a detailed comparison of experimental and calculated data. In future work we will take a look on the role of different basis sets on the frontier orbitals compositions and derive EPR parameters out of the DFT calculations.

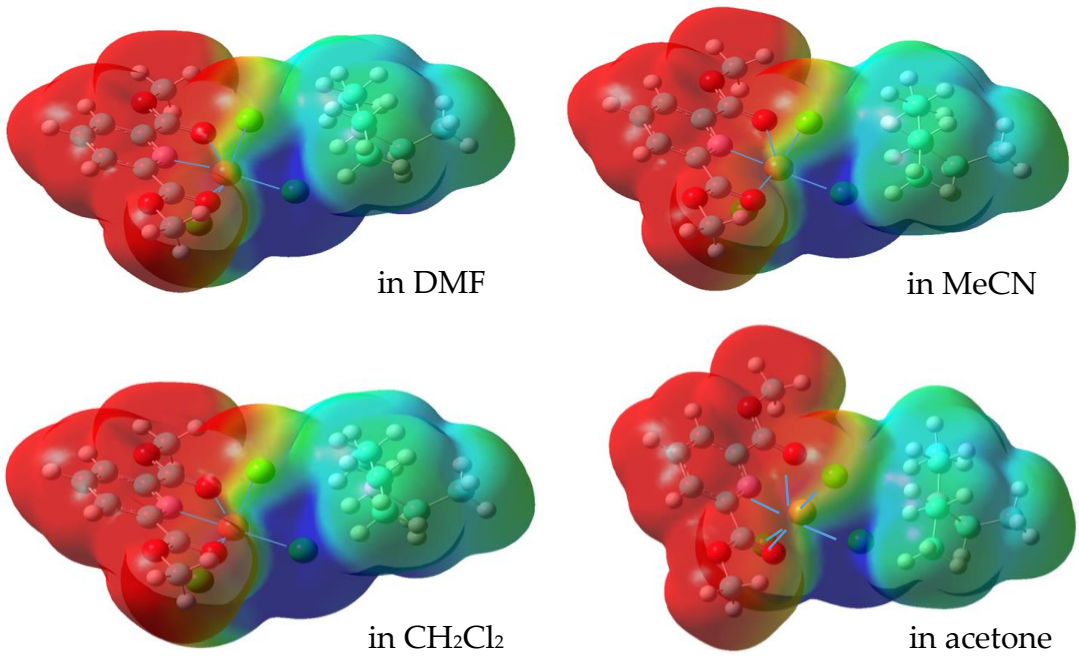

Figure S9. Electrostatic potential maps of $(HNEt_3)[Cu(pydicMe_2)Cl_3]$ in solvent media. Contours are color-coded from red (negative) to blue (positive).

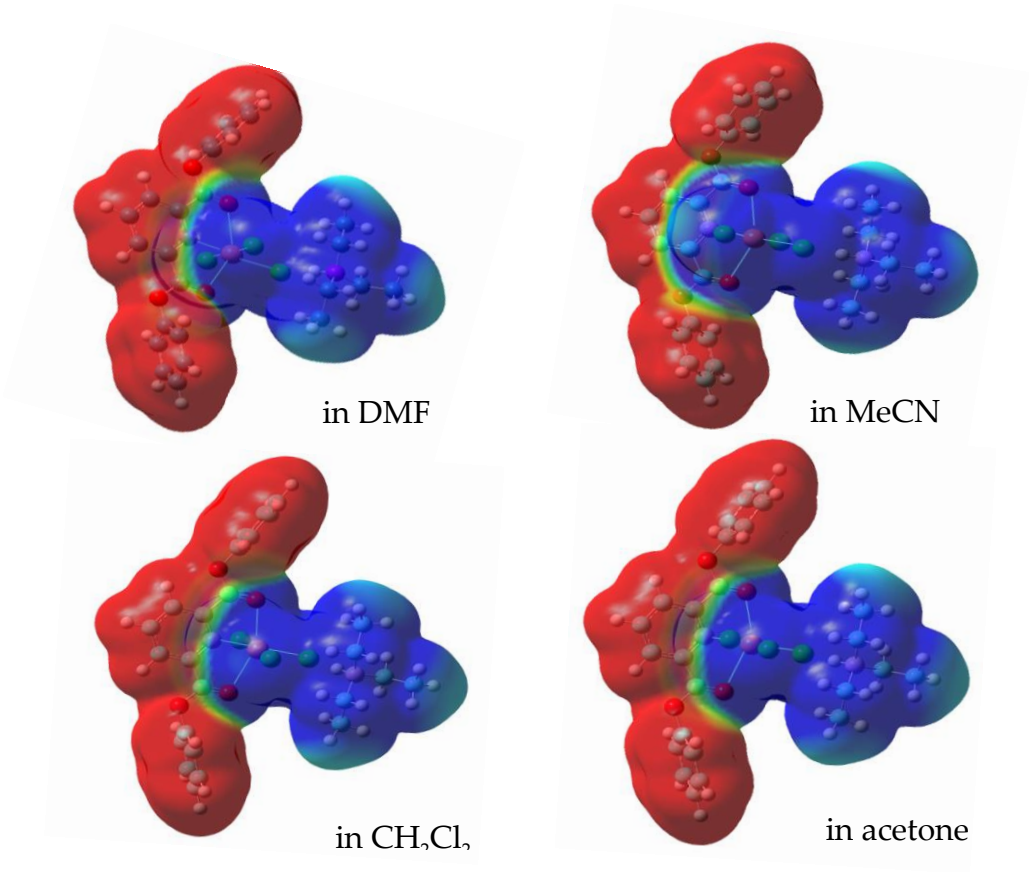

Figure S10. Electrostatic potential maps of $(HNEt_3)[Cu(pydicPh_2)Cl_3]$ in the solvent media. Contours are color-coded from red (negative) to blue (positive).

Supporting Tables:

Table S1. Crystal structure and refinement data of copper complexes and the ligand pydic(IPh)$_2$. [a]

	$[Cu(OH_2)_6][\{Cu(pydic)\}_2(\mu\text{-}Cl)_2]$	$(HNEt_3)[Cu(pydicMe_2)Cl_3]$	pydic(IPh)$_2$
formula	$C_{14}H_{18}Cl_2Cu_3N_2O_{14}$	$C_{15}H_{25}N_2O_4Cl_3Cu$	$C_{19}H_{11}I_2NO_4$
f. w. /g mol^{-1}	671.73	467.26	571.09
crystal shape	needle	plate	block
colour	turquoise	green-brown	colourless
crystal system	triclinic	triclinic	orthorhombic
space group	$P\bar{1}$ (No. 2)	$P\bar{1}$ (No. 2)	*P*bca (No. 61)
a /Å	8.185(3)	7.706(5)	13.520(5)
b /Å	9.500(3)	10.274(5)	14.455(5)
c /Å	9.682(2)	13.666(5)	19.496(5)
α /°	69.01(3)	93.846(5)	90
β /°	66.97(3)	92.271(5)	90
γ /°	89.04(4)	107.216(5)	90
volume /Å^3, Z	640.2(4), 1	1029.1(9), 2	3810(2), 8
F(000)	337	482	2160
density / g cm^{-1}	1.784	1.508	1.991
abs. coeff / mm^{-1}	2.742	1.471	3.325
refl. coll.	7681	12435	34795
data / restr. / param.	2849 / 0 / 160	4604 / 0 / 233	4654 / 0 / 235
h, k, l,	$-10 < h < 10$	$-9 < h < 10$	$-17 < h < 17$
	$-12 < k < 12$	$-13 < k < 13$	$-19 < k < 19$
	$-12 < l < 12$	$-18 < l < 18$	$-25 < l < 25$
Goof on F^2	1.015	0.684	0.739
R_{int}	0.0658	0.1258	0.0939
final *R* indices	$R1 = 0.0813$	$R1 = 0.0399$	$R1 = 0.0329$
[I>2σ(I)]	$wR2 = 0.2361$	$wR2 = 0.0524$	$wR2 = 0.0522$
R indices (all data)	$R1 = 0.1291$	$R1 = 0.1467$	$R1 = 0.1272$
	$wR2 = 0.2593$	$wR2 = 0.0688$	$wR2 = 0.0671$
largest diff. p. a. h. /e Å^{-3}	3.793 and −1.489	0.359 and −0.315	0.437 and −0.597
CCDC	1878792	1878795	1878792

[a] The measurements were performed at 293(2) K using graphite-monochromatized Mo-Kα radiation (λ = 0.71073 Å). The structures were solved by direct methods using SHELX-97 and WinGX (SHELXS-97) [1,2,3] and refined by full-matrix least-squares techniques against F^2 (SHELXL-2017/1) [4,5]. The numerical absorption corrections (X-RED V1.22; Stoe & Cie, 2001) were performed after optimising the crystal shapes using X-SHAPE V1.06 (Stoe & Cie, 1999) [6,7]. The non-hydrogen atoms were refined with anisotropic displacement parameters. H atoms were included by using appropriate riding models.

Table S2. DFT-calculated structure parameters for mononuclear $[Cu(pydic(IPh)_2)Cl_2]$ and binuclear $[\{Cu(pydic(IPh)Cl\}_2(\mu\text{-}Cl)_2]$.[a]

	$[Cu(pydic(IPh)_2)Cl_2]$	$[\{Cu(pydic(IPh)_2)Cl\}_2(\mu\text{-}Cl)_2]$.
Cu···Cu	-	3.566
$Cu–Cl_{(eq)}$	2.151	2.320
$Cu–Cl_{(ax)}$	2.247	2.235
$Cu–Cl_{(\mu\text{-}ax)}$	-	2.426
Cu–N	2.128	2.109
Cu–O1	2.503	2.496
Cu–O2	2.510	2.609
C=O1	1.203	1.201

C=O2	1.203	1.200
N–Cu–$Cl_{(eq)}$	153.2	162.3
N–Cu–$Cl_{(ax)}$	88.4	98.4
N–Cu–$Cl_{(\mu\text{-}ax)}$	-	85.7

[a] Calculated at def-SV(P)/B3LYP level using TMoleX [8,9].

Table S3. DFT-calculated structure parameters for $(HNEt_3)[Cu(pydicR_2)Cl_3]$ (R = Me or Ph) in the gas phase.[a]

	$(HNEt_3)[Cu(pydicMe_2)Cl_3]$	$(HNEt_3)[Cu(pydicPh_2)Cl_3]$
Cu-Cl1	2.37	2.37
Cu-Cl2	2.32	2.31
Cu-Cl3	2.29	2.30
Cu-O1	2.60	2.61
Cu-O2	2.49	2.50
Cu-N1	2.14	2.15
Cl2…H_{22}	2.01	2.03
Cl1…H_{22}	2.98	2.98

[a] Calculated at 6-31+g(d,P)/B3LYP level using Gaussian09 [10].

Table S4. DFT-calculated structure parameters for $(HNEt_3)[Cu(pydicR_2)Cl_3]$ (R = Me or Ph) in CH_2Cl_2 as solvent.[a]

	$(HNEt_3)[Cu(pydicMe_2)Cl_3]$	$(HNEt_3)[Cu(pydicPh_2)Cl_3]$
Cu-Cl1	2.37	2.37
Cu-Cl2	2.33	2.32
Cu-Cl3	2.35	2.35
Cu-O1	2.51	2.51
Cu-O2	2.49	2.51
Cu-N1	2.11	2.11
Cl2…H_{22}	2.16	2.17
Cl1…H_{22}	3.16	3.15

[a] Calculated at 6-31+g(d,P)/B3LYP level applying the polarised continuum model (PCM) in Gaussian09 [10].

Table S5. DFT-calculated structure parameters for $(HNEt_3)[Cu(pydicR_2)Cl_3]$ (R = Me or Ph) in acetone as solvent.[a]

	$(HNEt_3)[Cu(pydicMe_2)Cl_3]$	$(HNEt_3)[Cu(pydicPh_2)Cl_3]$
Cu-Cl1	2.37	2.37
Cu-Cl2	2.33	2.32
Cu-Cl3	2.36	2.36
Cu-O1	2.51	2.51
Cu-O2	2.49	2.51
Cu-N1	2.10	2.11
Cl2…H_{22}	2.20	2.22
Cl1…H_{22}	3.16	3.08

[a] Calculated at 6-31+g(d,P)/B3LYP level applying the polarised continuum model (PCM) in Gaussian09 [10].

Table S6. DFT-calculated structure parameters for $(HNEt_3)[Cu(pydicR_2)Cl_3]$ (R = Me or Ph) in MeCN as solvent.[a]

	$(HNEt_3)[(pydicMe_2)CuCl_3]$	$(HNEt_3)[(pydicPh_2)CuCl_3]$
Cu-Cl1	2.37	2.37
Cu-Cl2	2.33	2.32

Cu-Cl3	2.36	2.36
Cu-O1	2.50	2.51
Cu-O2	2.49	2.51
Cu-N1	2.10	2.10
Cl2…H_{22}	2.21	2.23
Cl1…H_{22}	3.16	3.08

[a] Calculated at 6-31+g(d,P)/B3LYP level applying the polarised continuum model (PCM) in Gaussian09 [10].

Table S7. DFT-calculated structure parameters for $(HNEt_3)[Cu(pydicR_2)Cl_3]$ (R = Me or Ph) in DMF as solvent.[a]

	$(HNEt_3)[(pydicMe_2)CuCl_3]$	$(HNEt_3)[(pydicPh_2)CuCl_3]$
Cu-Cl1	2.37	2.37
Cu-Cl2	2.33	2.32
Cu-Cl3	2.37	2.36
Cu-O1	2.51	2.51
Cu-O2	2.49	2.51
Cu-N1	2.10	2.10
Cl2…H_{22}	2.22	2.23
Cl1…H_{22}	3.16	3.08

[a] Calculated at 6-31+g(d,P)/B3LYP level applying the polarised continuum model (PCM) in Gaussian09 [10].

Table S8. DFT-calculated second-order perturbation energies $E^{(2)}$ (kJ/mol) of selected orbital interactions in $(HNEt_3)[(pydicPh_2)CuCl_3]$ in the gas phase and solvents.[a]

donor	acceptor	gas phase	CH_2Cl_2	acetone	MeCN	DMF
LP*(8) Cu1	BD*(1) N2–H22	21.30	9.21	8.03	7.66	7.66
LP(1) Cl1	LP*(7) Cu1	50.63	51.71	52.55	52.93	52.97
LP(4) Cl1	LP*(6) Cu1	101.92	99.87	100.08	100.46	100.46
LP(4) Cl1	LP*(7) Cu1	169.12	180.92	182.38	183.09	183.13
LP(1) Cl2	LP*(8) Cu1	63.43	59.12	59.83	59.71	59.71
LP(4) Cl2	LP*(6) Cu1	108.41	102.47	125.65	126.27	126.32
LP(4) Cl2	LP*(8) Cu1	157.24	160.12	159.87	159.54	159.49
LP(3) Cl2	BD*(1) N2-H22	65.56	48.33	40.67	39.04	38.95
LP(1) Cl3	LP*(7) Cu1	73.72	64.31	63.64	63.51	63.51
LP(4) Cl3	LP*(6) Cu1	119.62	105.48	103.51	102.84	102.80
LP(4) Cl3	LP*(7) Cu1	204.47	192.00	191.13	190.75	190.75
LP(1) O1	LP*(9) Cu1	31.34	36.07	35.94	36.02	36.02
LP(1) O2	LP*(9) Cu1	36.36	34.98	35.94	36.02	36.02
LP(1) N1	LP*(6) Cu1	64.64	70.63	71.42	71.71	71.71
LP(1) N1	LP*(8) Cu1	63.30	70.08	71.46	71.92	71.95

[a] LP = lone pairs, BD* = antibonding orbitals. Calculated at 6-31+g(d,P)/B3LYP level and applying the polarised continuum model (PCM) in Gaussian09 [10].

Supporting Experimental:

Structure solution and description of structural details of $pydic(IPh)_2$.

Single crystals of pydic(IPh)$_2$ suitable for XRD were obtained from acetone solutions by slow evaporation and the structure was solved in the orthorhombic space group *P*bca (details in Table S1). The molecular structure depicted in Figure S1 shows the ligand providing a binding pocket for the formation of **CC** isomeric complexes as recently also reported for the pydicMe$_2$ derivative [11]. The planes of both phenol rings are tilted away from the pyridine ring (61° and 64°) one iodo substituent is located above the pyridine ring plane, while the other resides beneath this plane. The two carbonyl functions are slightly tilted from the pyridine plane, each pointing in the same direction as the iodo substituent of the corresponding phenol ring. The conformation might result from packing effects in the crystal leading to the formation of π-stacked dimers (Figure S1). Additionally, the iodo substituents of the molecules are pointing towards each other with an I···I distance of only 4.350(1) Å, thus forming dimers while relevant H bridges are missing in the crystal structure.

Structure solution and description of structural details of [Cu(OH$_2$)$_6$][{Cu(pydic)}$_2$(μ-Cl)$_2$].

crystals of [Cu(OH$_2$)$_6$][{Cu(pydic)}$_2$(μ-Cl)$_2$] were obtained by slow evaporation of a methanolic solution. The crystal structure was solved and refined in the triclinic space group $P\bar{1}$ (details in Table S1). The structure reveals the complex cation [Cu(OH$_2$)$_6$]$^{2+}$ and a centrosymmetric binuclear μ-chlorido bridged dianionic complex [{Cu(pydic)}$_2$(μ-Cl)$_2$]$^{2-}$. [Cu(OH$_2$)$_6$]$^{2+}$ can be described as an axially elongated octahedral coordination (Cu2−O5 = 1.979(9) Å; Cu2−O6 = 1.965(9) Å and Cu2−O11 = 2.53(2) Å), in line with previous reports on related compounds [12,13]. The dianion [{Cu(pydic)}$_2$(μ-Cl)$_2$]$^{2-}$ shows a distorted square pyramidal geometry around each copper atom. With a short equatorial bond Cu−Cl$_{eq}$ = 2.212(4) Å and a long axial bond Cu−Cl$_{ax}$ = 2.692(3) Å, while the Cu−N bond is rather short (1.93(1) Å). Both pydic^{2-} ligands are completely coplanar.

References

[1] G. M. Sheldrick, A short history of SHELX. *Acta Crystallogr., Sect. A: Found. Crystallogr.*, **2008**, *64*, 112–122.

[2] G. M. Sheldrick, SHELX-97, Programs for Crystal Structure Analysis, Göttingen, 1997.

[3] L. J. Farrugia, WinGX and ORTEP for Windows: an update. *J. Appl. Cryst.* **2012**, *45*, 849–854.

[4] G. M. Sheldrick, SHELXL-2017/1, Program for the Solution of Crystal Structures, University of Göttingen, Germany, 2017.

[5] G. M. Sheldrick, Crystal structure refinement with SHELXL. *Acta Crystallogr., Sect. C: Struct. Chem.*, **2015**, *71*, 3–8.

[6] STOE X-RED, Data Reduction Program, Version 1.22/Windows, STOE & Cie, Darmstadt, Germany 2001.

[7] STOE X-SHAPE, Crystal Optimisation for Numerical Absorption Correction, Version 1.06/Windows, STOE & Cie, Darmstadt, Germany 1999.

[8] TURBOMOLE 7.0, TURBOMOLE GmbH, Karlsruhe, Germany 2015.

[9] C. Steffen, K. Thomas, U. Huniar, A. Hellweg, O. Rubner, A. Schroer, TmoleX-a graphical user interface for TURBOMOLE. *J. Comput. Chem.* **2010**, *31*, 2967–2970.

[10] M. J. Frisch, G. W. Trucks, H. B. Schlegel, G. E. Scuseria, M. A. Robb, J. R. Cheeseman, G. Scalmani, V. Barone, B. Mennucci, G. A. Petersson, et. al., Gaussian Inc, Wallingford CT, USA 2009.

[11] J.-Y. Huang, W. Xu, Dimethyl pyridine-2,6-dicarboxylate, *Acta Cryst. Sect. E.* **2006**, *62*, o2653–o2654.

[12] T. Glowiak, I. Podgórska, X-ray, Spectroscopic and Magnetic Studies of Hexaaquacopper(II) Di(diphenylphosphate) Diglycine, *Inorg. Chim. Acta* **1986**, *125*, 83–88.

[13] M. V. Kirillova, M. F. C. Guedes da Silva, A. M. Kirillov, J. J. R. Fraústo da Silva, A. J. L. Pombeiro, 3D hydrogen bonded heteronuclear Co^{II}, Ni^{II}, Cu^{II} and Zn^{II} aqua complexes derived from dipicolinic acid, *Inorg. Chim. Acta* **2007**, *360*, 506–512.